

MOA 2003-BLG-37: A Bulge Jerk-Parallax Microlens Degeneracy

B.-G. Park¹, D.L. Depoy², B.S. Gaudi³, A. Gould², C. Han^{2,4}, and R.W. Pogge²

(The FUN Collaboration)

and

F. Abe⁵, D.P. Bennett⁶, I.A. Bond⁷, S. Eguchi⁵, Y. Furuta⁵, J.B. Heamshaw⁸, K. Kamaya⁵,
P.M. Kilmer⁸, Y. Kurata⁵, K. Masuda⁵, Y. Matsubara⁵, Y. Muraki⁵, S. Noda⁹, K.
Okajima⁵, N.J. Rattenbury¹⁰, T. Sako⁵, T. Sekiguchi⁵, D.J. Sullivan¹¹, T. Sumi¹², P.J.

Tristram¹⁰, T. Yanagisawa¹³, and P.C.M. Yock¹⁰

(The MOA Collaboration)

ABSTRACT

¹Korea Astronomy Observatory, 61-1, W haam -Dong, Youseong-Gu, Daejeon 305-348, Korea; bg-park@boao.re.kr

²Department of Astronomy, The Ohio State University, 140 West 18th Avenue, Columbus, OH 43210, USA; depoy, gould, pogge@astronomy.ohio-state.edu

³Harvard-Smithsonian Center for Astrophysics, Cambridge, MA 02138, USA; sgaudi@cfa.harvard.edu

⁴Department of Physics, Institute for Basic Science Research, Chungbuk National University, Chongju 361-763, Korea; cheongho@astroph.chungbuk.ac.kr

⁵Solar-Terrestrial Environment Laboratory, Nagoya University, Nagoya 464-8601, Japan; abe, furuta, kkamaya, km asuda, kurata, muraki, oka jima, sado, sako, sekiguchi, ymatsu@stelab.nagoya-u.ac.jp

⁶Department of Physics, Notre Dame University, Notre Dame, IN 46556, USA; bennett@nd.edu

⁷Institute for Astronomy, University of Edinburgh, Edinburgh, EH 9 3HJ, UK; iab@roe.ac.uk

⁸Department of Physics and Astronomy, University of Canterbury, Private Bag 4800, Christchurch, New Zealand; john.heatshaw, pam.kilmer@canterbury.ac.nz

⁹National Astronomical Observatory of Japan, Tokyo, Japan; sachit.noda@nao.ac.jp

¹⁰Department of Physics, University of Auckland, Auckland, New Zealand; nrat001@phy.auckland.ac.nz, paulonika@hotmail.com, p.yock@auckland.ac.nz

¹¹School of Chemical and Physical Sciences, Victoria University, PO Box 600, Wellington, New Zealand; denis.sullivan@vuw.ac.nz

¹²Department of Astrophysical Sciences, Princeton University, Princeton NJ 08544, USA; sumi@astro.princeton.edu

¹³National Aerospace Laboratory, Tokyo, Japan; tyaniagi@nsl.go.jp

We analyze the Galactic bulge microlensing event MOA 2003-BLG-37. Although the Einstein timescale is relatively short, $t_E = 43$ days, the lightcurve displays deviations consistent with parallax effects due to the Earth's accelerated motion. We show that the χ^2 surface has four distinct local minima that are induced by the "jerk-parallax" degeneracy, with pairs of solutions having projected Einstein radii, $r_E = 1.76$ AU and 1.28 AU, respectively. This is the second event displaying such a degeneracy and the first toward the Galactic bulge. For both events, the jerk-parallax formalism accurately describes the offsets between the different solutions, giving hope that when extra solutions exist in future events, they can easily be found. However, the morphologies of the χ^2 surfaces for the two events are quite different, implying that much remains to be understood about this degeneracy.

Subject headings: gravitational lensing

1. Introduction

Microlens parallaxes are playing an increasingly important role in the analysis of microlensing events. The microlens parallax, π_E is a vector, whose magnitude is the ratio of the size of the Earth's orbit (1 AU) to the Einstein radius projected onto the plane of the observer ($r_E = \text{AU} = \pi_E$), and whose direction is that of the lens-source relative motion. From simple geometrical considerations (e.g., Gould 2000),

$$\pi_E = \frac{r_{\text{rel}}}{M}; \quad \pi_E = \frac{P}{M_{\text{rel}}}; \quad \frac{4G}{c^2 \text{AU}} \approx 8.1 \frac{\text{mas}}{M}; \quad (1)$$

where M is the mass of the lens, r_{rel} is the lens-source relative parallax, and π_E is the angular Einstein radius. Hence, if both π_E and μ_E can be measured, one can determine both M and r_{rel} . While this has only been done for one microlensing to date (An et al. 2002), there are plans to apply this technique to several hundred events using the Space Interferometry Mission (SIM) (Gould & Salim 1999).

Moreover, even in cases for which π_E cannot be measured, the microlens parallax can give very important information about the event. When combined with the Einstein timescale, t_E , it yields v , the lens-source relative velocity projected onto the observer plane,

$$v = \frac{\pi_E}{t_E} \frac{\text{AU}}{c}: \quad (2)$$

By combining measurements of μ_E and t_E with known Galactic structure parameters, Mao et al. (2002) and Bennett et al. (2002) were able to show that several microlensing events seen toward the Galactic bulge are most probably due to black holes.

Microlens parallax measurements are possible whenever π_E can be compared to some "standard ruler" in the observer plane. The two logical possibilities are observing the event simultaneously from two different locations and observing the event from an accelerated platform. Since π_E is typically of order an AU, the most practical realizations of these ideas would be, respectively, to observe the event simultaneously from a satellite in solar orbit (Refsdal 1966) and (for sufficiently long events) to observe it from the Earth as it moves about the Sun (Gould 1992).

When Refsdal (1966) first proposed obtaining microlens parallaxes by combining space-based and ground-based observations of microlensing events, he already noted that these measurements would generically be subject to an ambiguity. Using somewhat different notation, he showed that,

$$\mu_E(\mu_k; \mu_{\perp}) = \frac{AU}{d_{\text{sat}}}(\mu_k; u_0) \quad (3)$$

where d_{sat} and the parallel (k) direction are defined by the magnitude and direction of the Earth-satellite separation vector projected onto the plane of the sky, $\mu_{\perp} = t_0 - t_E$ is the difference in times of maximum, t_0 , as seen from the Earth and satellite (normalized to t_E), and u_0 is the difference in impact parameters. While μ_k (and so $\mu_E(\mu_k)$) is unambiguously defined,

$$u_0 = \pm \sqrt{u_{\text{sat}}^2} \quad (4)$$

and so μ_{\perp} is subject to a two-fold degeneracy in magnitude, depending on whether the event impact parameters u_0 register the lens passing on the same (−) or opposite (+) sides of the lens as seen from the Earth and satellite. And μ_{\perp} is subject to an additional two-fold ambiguity in sign, depending on the relative orientations of these separations. See Gould (1995) for a fuller discussion of this degeneracy.

Although no space-based parallaxes have ever been measured, this degeneracy and the conditions under which it can be broken have been the subject of a great deal of theoretical work (Gould 1995; Bouché & Gould 1996; Gaudi & Gould 1997; Gould & Salim 1999). By contrast, despite the fact that more than a dozen microlens parallaxes have been measured using the Earth's motion (Alcock et al. 1995, 2001; Mao 1999; Soszynski et al. 2001; Bond et al. 2001; Smith, Mao & Wozniak 2002; Mao et al. 2002; An et al. 2002; Bennett et al. 2002; Smith, Mao & Paczynski 2003), the existence of a discrete microlens parallax degeneracy for the case of an accelerated observer was not discovered until the past year (Smith et al. 2003), and the fact that there is actually a four-fold discrete degeneracy that is analogous

to equation (3) was only just recently recognized (Gould 2004).

One reason for this late development is that the discrete degeneracy is typically broken for long events, $t_E \gg 1$, where 1 yr^{-1} . However, this cannot be the full explanation; Smith et al. (2003) showed that some previously analyzed events had unrecognized discrete degeneracies, and the first analysis of a four-fold degeneracy came 10 years after the event was discovered. Another reason, perhaps, is that while the four-fold degeneracy assumes a relatively simple form in the geocentric frame (Gould 2004), all previous parallax analyses were carried out in the heliocentric frame, in which it is much more difficult to recognize the physical symmetries that underlie this degeneracy.

Whatever the exact reason for their prior neglect, it is important now to gain a better understanding of discrete parallax degeneracies, which are expected to be significant primarily in events that have good data and that lie below the threshold $t_E \approx 1$. For cases in which this degeneracy can be resolved by an independent measurement of the lens-source relative proper motion (e.g., Alcock et al. 2001), it will be possible to measure the lens mass and distance. Moreover, Gould (1999) showed that the degeneracies in space-based and Earth-based parallax measurements are complementary, so that the full microlens parallax can sometimes be recovered by combining these even when each measurement is separately degenerate. This will have practical applications to the SIM mission, which has a major microlensing component. Finally, the parallax effects in the relatively short events that can give rise to a discrete degeneracy can also be confused with some signatures of planetary companions to the lens (Gaudi et al. 2002). An understanding of this degeneracy is therefore required for a proper analysis of microlensing planet searches.

There are strong, although not perfect, analogies between the space-based discrete parallax degeneracy first analyzed by Refsdal (1966) and the Earth-based degeneracy. In both cases, there is a preferred (k) axis, and the parallax component along this axis, $\pi_{E,k}$ is hardly affected by the degeneracy. For the space-based case, this axis is the Earth-satellite separation vector, while for the Earth-based case it is the direction of the Sun's apparent acceleration (in the geocentric frame). In both cases, there is a two-fold degeneracy that basically does not affect the magnitude of π_E . For the space-based case, this is due to the first \backslash " in equation (4) and corresponds to a parity flip of the entire event, with the lens reversing the side it passes the source as seen from both the Earth and the satellite. For the Earth-based case, this two-fold degeneracy takes $u_0 \rightarrow -u_0$ and so also corresponds to the lens reversing the side it passes the source. Finally, in both cases, there is an additional two-fold degeneracy that does affect the magnitude of π_E . For the space-based case, this is due to the second \backslash " in equation (4) and corresponds to the lens passing on the same versus the opposite side of the source as seen from the Earth and satellite. For the Earth-based

case, this degeneracy can be expressed in terms of the so-called "jerk parallax",

$$j = \frac{4}{3} \frac{j}{a_E^2 t_E}; \quad (5)$$

where a_E is the (2-dimensional) acceleration of the Sun in the Earth frame projected onto plane of the sky and divided by an AU, and where $j = d^3u/dt^3$ is the jerk. The degeneracy arises because event geometries with the same fourth-order Taylor coefficient of the lens-source separation,

$$C_4 = \frac{1}{4} (a_E^2 + j t_E^2) + \frac{1}{12} u_0^2 t_E^{-2}; \quad (6)$$

will, to this order, generate the same lightcurve. Hence, in the limit $j u_0 \rightarrow 1$, if a_E is one solution, then a_E^0 , with

$$a_{E,jk}^0 = a_{E,jk}; \quad a_{E,j?}^0 = (a_{E,j?}^2 + j_{j?}^2 t_E^2); \quad (7)$$

is also a solution.

While theoretical investigations are essential for understanding the jerk-parallax degeneracy, it is also important to analyze individual degenerate events. In particular, Gould (2004) predicted that the phenomenology of this degeneracy should be much richer for events observed toward the Galactic bulge than for those seen toward the Large Magellanic Cloud (LMC) because the bulge lies near the ecliptic while the LMC lies near the ecliptic pole. The jerk-parallax can be reexpressed in terms of a projected velocity,

$$v_j = \frac{AU}{j_{j?}^2 t_E} = \frac{3}{4} \frac{^3AU}{j_{j?}^2}; \quad (8)$$

which (approximating the Earth's orbit as circular) can be evaluated,

$$v_j = \frac{3 (\cos^2 \delta + \sin^2 \delta \cos^2 \phi)^{3/2}}{4 \sin \delta} v; \quad (9)$$

Here δ is the ecliptic latitude, ϕ is the phase of the Earth's orbit relative to opposition, and $v = 30 \text{ km s}^{-1}$ is the speed of the Earth. (Note that $j_{j?}$ is a signed scalar.) Toward the LMC (near the ecliptic pole), $v_j \approx 22 \text{ km s}^{-1}$, independent of the time of year. However, toward the bulge (near the ecliptic), v_j varies from a factor $\sin^2 \delta$ below this value to $j \cos^2 \delta$ above it. Since v_j characterizes the jerk-parallax degeneracy through equations (7) and (8), the bulge's much broader range of values for this parameter implies a broader range of phenomena.

Here we analyze MOA 2003-BLG-37, the first bulge microlensing event whose parallax solution has four distinct minima. We show that the analytic formalism developed by Gould (2004) to describe the jerk parallax applies quite well to this event. However, the morphology of the 2 contours of this event is very different from that of MACHO-LMC-5, the only other event for which the jerk-parallax degeneracy has been detected.

2. Data

MOA 2003-BLG-37 [(RA, DEC) = (18:12:22.4, -29:01:01.3), (l, b) = (3:152; -5:656)] was alerted by the Microlensing Observations for Astrophysics (MOA) collaboration on 2003 June 24 as part of its ongoing alert program (Bond et al. 2001) when the lens was about 1.5 Einstein radii from the source. MOA obtained a total of 626 observations in I band using the 0.6 m Boller & Chivens telescope at Mt. John University Observatory in New Zealand. Of these, 359 observations were during the 2003 season and the remaining 269 were during 3 previous seasons. The data were reduced using on-line image subtraction.

The Microlensing Follow Up Network (FUN, Yoo et al. 2004) commenced observations approximately two weeks before the peak, which occurred on HJD⁰ - HJD - 2450000 = 2880:68 (UT 2003 August 29.18), using the ANDICAM camera on the 1.3m SMARTS (former 2MASS) telescope at Cerro Tololo Interamerican Observatory at La Serena, Chile. FUN obtained 116 observations in I and 13 in V. The photometry was carried out using DOPHOT (Schechter, Mateo & Saha 1993). ANDICAM is equipped with an optical/IR dichroic beam splitter, allowing H band observations to be taken simultaneously with each optical image. However, the H band data show much larger scatter than the optical data, and so their incorporation does not significantly affect the solution nor reduce the errors. Hence, we exclude them.

After the event peaked, we realized that it might have a measurable parallax, and we therefore made special efforts to observe the event regularly until late in the season so as to obtain good coverage of its falling wing. Since the Sun's acceleration projected on the plane of the sky reaches a maximum on about Sept 24 (roughly 0.6 Einstein radii after peak), the falling wing is the most sensitive to parallax. Observations continued several times per week until the end of October at both observatories. Reported errors at both observatories were typically 0.01 to 0.02 mag near baseline and smaller near the peak.

Of the 626 MOA points, four were found to be mild ($\sim 3.5\sigma$) outliers and were eliminated from the analysis. The MOA errors were renormalized upward by a factor 1.47 in order to make their χ^2 per degree of freedom (dof) consistent with unity. The FUN I and V data did not contain any outliers greater than 3σ , and their χ^2/dof were both consistent with unity, so no adjustments were applied.

3. Event Characteristics

The lightcurve was initially fit to a point-source point-lens (PSP/L) Paczynski (1986) model, the parameters for which are shown in Table 1. It is a relatively high-magnification

event, with maximum magnification $A_{\text{max}} = 20$. The data generally cover the lightcurve quite well. See Figure 1. Figure 2 is an instrumental color-magnitude diagram (CMD) of the eld, which is based on FUN V and I data, that has been translated so that the centroid of the bulge clump (marked by a cross) lies at its known position (Yoo et al. 2004), $[I_0; (V - I)]_{\text{clump}} = (14.32; 1.00)$. For stars that lie behind the disk reddening screen, the diagram therefore shows their dereddened color and magnitude, while foreground stars that lie within the dust distribution (e.g., the "reddening sequence" toward the upper left) appear in the diagram as brighter and bluer than they actually are. The dereddened color and magnitude of the microlensed source (when unmagnified) are shown as an open circle. These values are determined from the fits for the deblended source fluxes f_s in V and I from FUN, i.e., the same data set used to construct the CMD. Using jackknife, we find that the statistical errors from centroiding the clump are 0.02 mag in each axis. The entire procedure assumes a uniform reddening over the $6^\circ \times 6^\circ$ eld. In fact, we find that when we consider stars within $100''$ of the source star (and so shrink the sample size by 75%), the clump centroid shifts by only 0.02 mag in color and 0.05 mag in brightness, which are both consistent with statistical fluctuations. That is, there is no evidence for differential reddening on the relevant scales.

Based on its position in the CMD, the source could be a clump giant in the bulge but it could equally well be a disk first-ascent giant that lies ~ 1 mag in the foreground. We determine the angular size of the source from its position on the instrumental CMD using the standard approach as summarized by Yoo et al. (2004). Very briefly, we use standard color-color relations to convert the observed $(V - I)_0 = 0.91$ to $(V - K)_0 = 2.06$. Then using the dereddened $V_0 = 15.27$ and the van Belle (1999) empirical color/surface-brightness relation, we find,

$$\theta = 5.8 \pm 0.5 \text{ as} \quad (10)$$

The error is almost entirely due to the 8.7% scatter in the van Belle (1999) relation. The next largest source of error comes from the 0.07 mag uncertainty in the fit to the source flux, which contributes about 3% in quadrature to θ . Other sources, such as the 0.004 mag error in the fit color and the 0.02 mag errors in the color and magnitude of the clump centroid, contribute still less. The total error is 9.5%. (Note that this entire procedure rests on instrumental magnitudes, so absolute calibration of the photometry is not necessary.)

We consider finite-source effects, holding $\mu = \mu_E$ at various values while fitting for the other parameters. We find a minimum $\chi^2 = 751.37$ at $\mu = 0.023$, but since this is only $\chi^2 = 1.7$ lower than at $\mu = 0$ (see Table 1), we do not consider this to be a significant detection of finite-source effects. We are, however, able to put an upper limit on μ , and so a lower limit on $\mu_E = \mu - \mu_s$ and hence on the lens-source relative proper motion $\mu_{\text{rel}} = \mu_E = \mu_s$.

We find,

$$\mu < 0.034; \quad \theta_E > 170 \text{ mas}; \quad \mu > 1.5 \text{ mas yr}^{-1}; \quad (11)$$

at the 2 σ level. (At 3 σ , $\mu < 0.44$.) These constraints are of marginal interest. The typical proper motion expected for bulge-bulge lensing events is about 5 mas yr^{-1} , and for disk-bulge events it is about 8 mas yr^{-1} . Hence, only the low- μ part of parameter space is eliminated. Similarly, from equation (1) for θ_E , we obtain,

$$\frac{M}{M_\odot} \frac{\mu_{\text{rel}}}{25 \text{ mas}} > 0.15: \quad (12)$$

Hence, only the very low-mass lenses with very small lens-source separations are eliminated.

Microensing flux observations $F(t)$ are always fit to the form,

$$F(t) = f_s A(t) + f_b; \quad (13)$$

where $A(t)$ is the model magnification as a function of time, f_s is the baseline flux of the lensed source, and f_b is the background light within the point spread function (PSF) that does not participate in the microensing event. A somewhat unsettling feature of the PSPL model is that it has negative blending f_b in both I and V, which is detected at the 6 σ level and so cannot be due to ordinary statistical fluctuations. Logically, there are only three other possible explanations: a failure of the model to take account of some essential physics affecting the lightcurve, systematic errors in the photometry, or a "negative source of light" within the PSF.

The last explanation is not as absurd as it might appear. The dense star fields of the Galactic bulge contain a mottled background of upper-main-sequence and turnoff stars that lie below the detection limit. If the source happens to lie in a "hole" in this background, the fit to the blended flux will be negative. By comparing the negative blend fluxes, f_b , to the source fluxes f_s , and referencing this comparison to the CMD, we find that the "hole" has a dereddened color and magnitude of $(I-V, I)_{\text{hole}} \approx (17.1; 0.5)$, which is about the right color but somewhat too bright to be a turnoff star. The position of this "hole" is shown as a filled triangle in Figure 2.

While systematic errors are possible, it seems unlikely that they would affect the independently measured V and I photometry by similar amounts. The remaining possible explanation is an inadequate model. Since blending is even in time (about the event peak), it can easily be confused with other even effects. The two most obvious possibilities are finite-source effects and parallax. The above mentioned 1.3 σ "detection" of finite-source effects does indeed tend to reduce the negative blending, but by a negligible amount. The $\theta_{E,k}$ component of θ_E gives rise to a third-order term, which is asymmetric in time and hence

cannot be confused with blending. However, the \mathbf{E}_{\parallel} component gives rise to a fourth-order term, which can be confused with blending (Smith et al. 2003).

4. Parallax Fits

The lightcurve shows a very minor asymmetry, being slightly brighter than the model on the rising side and slightly fainter on the falling side. See Figure 1. This, together with the negative-blending problem described in §3, lead us to fit the lightcurve for parallax. We employ the geocentric formalism of Gould (2004). We minimize χ^2 using Newton's method, starting with the no-parallax solution as a seed. We find a solution whose χ^2 is lower by approximately 32, which we regard as significant. See Table 1. To find the corresponding, $u_0 < 0$ solution predicted by Smith et al. (2003), we adopt a seed solution with $u_0 = -u_0$ and with all other parameters the same as the $u_0 > 0$ solution. We find that χ^2 is minimized extremely close to this seed. The difference in χ^2 of these two solutions is less than 1. See Table 1.

4.1. Jerk-Parallax Predictions

To navigate the jerk-parallax degeneracy, we employ the formalism of Gould (2004). We first evaluate the acceleration and jerk of the Sun projected onto the plane of the sky at time t_0 . We use the method of An et al. (2002) to find the path of the Sun projected on the plane of the sky and take numerical derivatives to obtain in (north, east) coordinates,

$$\mathbf{a} = (0.060; 0.382) \text{ }^{\circ} \text{ s}^{-2}; \quad \mathbf{j} = (-0.075; 0.441) \text{ }^{\circ} \text{ s}^{-3}. \quad (14)$$

Hence, the solar acceleration points almost due east, with a position angle of 86° (north through east). Since \mathbf{a} determines the parallel direction, the southern $u_0 > 0$ solution for \mathbf{E} listed in Table 1 can be represented in the (k, \parallel) coordinate system as,

$$\mathbf{E} = (\mathbf{E}_k; \mathbf{E}_{\parallel}) = (-0.049; 0.568); \quad (15)$$

This explains why the parallax signature in Figure 1 is so weak. The component of \mathbf{E} parallel to the solar acceleration, which is what gives rise to the parallax asymmetry, is extremely small. This asymmetry arises from the third-order term in the Taylor expansion of the lens-source separation (Gould 2004). Since this is the lowest order affected by parallax, it is also the easiest to notice in the lightcurve (Gould, Miralda-Escudé & Bahcall 1994). The perpendicular component first enters at fourth order (Gould 2004) and therefore is much harder to recognize.

From equations (5), (8), and (14), we find

$$j_{\text{?}} = 0.274; \quad \text{or} \quad v_j = 147 \text{ km s}^{-1} : \quad (16)$$

Combining equations (7), (15), and (16), and then switching to (north, east) coordinates, we predict that the degenerate solution will lie at,

$$(\begin{smallmatrix} 0 \\ E, \text{north} \end{smallmatrix}; \begin{smallmatrix} 0 \\ E, \text{east} \end{smallmatrix}) = (0.843; \quad 0.009) \quad (\text{predicted}): \quad (17)$$

We begin with this as a seed, and find that χ^2 is minimized at $(\begin{smallmatrix} 0 \\ E, \text{north} \end{smallmatrix}; \begin{smallmatrix} 0 \\ E, \text{east} \end{smallmatrix}) = (0.788; \quad 0.023)$, which is quite close to the predicted value. See Table 1.

We perform a similar exercise for the $u_0 < 0$ solutions. We predict the degenerate solution will lie at $(\begin{smallmatrix} 0 \\ E, \text{north} \end{smallmatrix}; \begin{smallmatrix} 0 \\ E, \text{east} \end{smallmatrix}) = (0.863; \quad 0.017)$ whereas it is actually found at $(\begin{smallmatrix} 0 \\ E, \text{north} \end{smallmatrix}; \begin{smallmatrix} 0 \\ E, \text{east} \end{smallmatrix}) = (0.783; \quad 0.012)$. We conclude that the formalism predicts the location of the jerk-parallax degenerate solutions quite well, at least in this case.

Some geometrical insight into this procedure can be gained from Figure 3, below. According to equation (7), the midpoint of the two solutions should lie at

$$E_{\text{mid}} = \frac{E_{\text{?}} + \begin{smallmatrix} 0 \\ E \end{smallmatrix}}{2} = (\begin{smallmatrix} 0 \\ E, \text{?} \end{smallmatrix}; \quad j_{\text{?}} = 2): \quad (18)$$

The first component says that both solutions (as well as their midpoint) should lie along a line defined by the Sun's apparent acceleration (labeled E_{jk} in the figure). This is indeed the case. The second component says that the midpoint should lie along this axis and $j_{\text{?}} = 2 = 0.137$ from the "perpendicular axis" (which is parallel to the arrow labeled $E_{\text{?}}$ and passes through the origin). This is also very nearly the case.

4.2. Timescale Predictions

The jerk-parallax formalism predicts that of the remaining parameters $(t_0; u_0; t_E; f_s; f_b)$, all but u_0 and t_E should be almost the same for all four solutions. Moreover, u_0 should only change sign, while t_E should differ among solutions by,

$$t_E \approx \frac{t_E^2}{2} (\begin{smallmatrix} 0 \\ E, \text{?} \end{smallmatrix} u_0 + u_0 \begin{smallmatrix} 0 \\ E, \text{?} \end{smallmatrix}) t_E : \quad (19)$$

Table 1 shows that these predictions are also borne out. The parameters t_0 , j_{10} , and the three sets of $(f_s; f_b)$ are all virtually unchanged among the four solutions. Equation (19) predicts $t_E = (0.60; 0.89; 0.46)$ days when comparing, respectively, the two southern, two northern, and corresponding southern and northern solutions. The actual differences from Table 1 are (0.62, 0.83, 0.70) days for the southern and northern pairs, and for the average of the two south/north comparisons, respectively.

4.3. Parallax Contours

To further explore the degeneracy, we calculate χ^2 for a grid of parallax values and show the resulting likelihood contours in Figure 3. There are three features to be noted. First, there are two local minima, which as discussed above are related to each other almost exactly as predicted by equation (7). Second, the northern minimum is higher by $\chi^2 = 7.5$ and so is formally excluded at the 2.6 level. See also Table 1. Third, each minimum is elongated along the $\mu_{E,?}$ axis and, indeed, is embedded in a larger continuous degeneracy also along this axis. That is, at the 4 level, there is a continuous set of acceptable solutions that extends almost from $\mu_{E,north} = -1$ to $\mu_{E,north} = 1$, but whose width is less than 0.005. The two discrete solutions form islands within this linear degeneracy.

5. Discussion

5.1. Comparison to MACHO-LMC-5

These three features should be contrasted to the case of MACHO-LMC-5, for which the analogous contour diagram is shown in Figure 3 of Gould (2004). For that event also, the jerk-parallax formalism accurately predicted (or rather postdicted) the location of the second minimum, and consequently the separation vector between the two solutions was perpendicular to the Sun-acceleration vector. However, in other respects the two cases are quite different. First, the two MACHO-LMC-5 minima had nearly identical χ^2 's. Second, these two minima were not severely elongated. Third, they did not lie within the continuous degeneracy.

In fact, Gould (2004) argued that there should be a hierarchy of microlens parallax degeneracies. When the data were adequate to solve for the source-lens separation only to second order in time, there would be no parallax information. When they were adequate to solve the separation to third order, there would be a continuous (linear) degeneracy. When they were adequate to solve to fourth order, the continuous degeneracy would be broken, but a discrete degeneracy would remain. Finally, if higher order terms could be measured, the degeneracy would be completely lifted. This picture would seem to argue that the discrete degeneracy should be embedded in the continuous degeneracy as it is in the present case of MOA 2003-BLG-37. It is curious therefore that for MACHO-LMC-5, the degeneracy is not embedded, even though it is more severe (in the sense the two minima have almost identical χ^2 's).

5.2. Negative Blending

After including parallax in the fit, negative blending remains in both V and I , but it is less severe. The dereddened color and magnitude of the "hole" is,

$$I_{0;\backslash\text{hole}}^{00} = 17.7 \pm 0.2; \quad (V - I)_{0;\backslash\text{hole}}^{00} = 0.2 \pm 0.3; \quad (20)$$

where the errors are approximately independent. The hole still has the right color (within errors) to be due to fluctuations in the turn-off-star background, and its amplitude is substantially smaller and so is consistent with an upper main-sequence or turn-off star. See Figure 2 (open triangle).

5.3. Xallarap

As Smith et al. (2003) point out, any lightcurve that can be fit by parallax can also be fit by xallarap (accelerated motion of the source). For long events with excellent data, the parallax parameters are so well determined that the putative xallarap solution can succeed in mimicking parallax only by having the source mirror the projected motion of the Earth to extremely high precision. In such cases, one may apply Occam's razor to argue that the xallarap solution is unlikely. For some other events, there may be external information that tends to corroborate the parallax interpretation, even if the parallax solution itself is not tightly constrained. For example, the lens of MACHO-LMC-5 was directly imaged which directly confirmed the direction of motion (Alcock et al. 2001) as well as the lens mass and distance (Gould 2004) derived from the parallax solution.

In the present case, the only auxiliary information comes from the constraint $\pi_E > 170 \mu\text{as}$, which was derived from the lack of finite-source effects. See equation (11). If the source is assumed to be at $D_s = 8 \text{ kpc}$, this implies that the Einstein radius projected on the source plane is $\hat{r}_E = D_{sE} \pi_E > 1.36 \text{ AU}$. To mimic the effect of the Earth's acceleration, the source must have a projected acceleration a_{sproj} such that $a_{sproj} \hat{r}_E = a_{proj} \hat{r}_E$, where $a_{proj} = \pi_E^2 \text{ AU}$ is the projected acceleration of the Earth. That is, $a_{sproj} = \hat{r}_E \pi_E^2 = \pi_E D_{sE} > 0.6a_\oplus$, where $a_\oplus = \text{AU yr}^{-2}$ is the (full) acceleration of the Earth. Such a source acceleration is of course possible. However, if such an acceleration were induced by a companion of mass m , then the velocity semi-amplitude would be at least $v > 23 (m/M_\odot)^{1/2} \text{ km s}^{-1}$. Hence, unless the companion were substellar or the system were seen pole on, it would be possible to detect such motion by radial velocity measurements.

6. Conclusions

We have shown that MOA 2003-BLG-37 suffers from a four-fold jerk-parallax degeneracy. The two pairs of solutions have microlens parallaxes of $\pi_E = 0.57$ and $\pi_E^0 = 0.78$. These correspond to projected Einstein radii of $r_E = 1.76 \text{ AU}$ and $r_E^0 = 1.28 \text{ AU}$. The first solution is favored at the 2:6 level. We were able to place only lower limits on the angular Einstein radius, $\theta_E > 170 \text{ } \mu\text{as}$. Combining the favored parallax measurement with this limit yield lower bounds on the mass and lens-source relative parallax of

$$M > 0.037 M_\odot ; \quad \pi_{\text{rel}} > 100 \text{ } \mu\text{as}; \quad (21)$$

neither of which probes a really interesting regime.

MOA 2003-BLG-37 is only the second event for which four separate minima have been found in χ^2 as a function of the vector microlens parallax π_E . The other was MACHO-LMC-5. For both events, the jerk-parallax formalism of Gould (2004) accurately predicts the position of the second pair of solutions given that the first pair has been found. This gives hope that the additional solution will easily be found in the future events that contain them.

On the other hand, there are substantial differences between the morphologies of the χ^2 contour diagrams for these two events in terms of the shapes and relative depths of the minima as well as the degree to which the minima are embedded in the lower-order continuous degeneracy. Further understanding of these differences is likely to require additional theoretical work as well as the study of additional events that display the jerk-parallax degeneracy. In particular, it would be useful to check all events with measured parallaxes to determine which of these are affected by this degeneracy. The black-hole candidates of Mao et al. (2002) and Bennett et al. (2002) would be especially interesting in this regard.

We thank the referee for making numerous comments and suggestions that significantly improved the paper. The MOA project is supported by the Marsden Fund of New Zealand, the Ministry of Education, Culture, Sports, Science and Technology (MEXT) of Japan, and the Japan Society for the Promotion of Science (JSPS). Work at OSU was supported by grants AST-02-01266 from the NSF and NAG-5-10678 from NASA. Work by CH was supported by the Astrophysical Research Center for the Structure and Evolution of the Cosmos (ARCSEC) of Korea Science & Engineering Foundation (KOSEF) through Science Research Program (SRC) program. Work by BGP was supported by Korea Astronomy Observatory (KAO).

REFERENCES

- Alcock, C., et al. 1995, *ApJ*, 454, L125
- Alcock, C., et al. 1997, *ApJ*, 486, 697
- Alcock, C., et al. 2001, *Nature*, 414, 617
- An, J.H., et al. 2002, *ApJ*, 572, 521
- Bennett, D.P., et al. 2002, *ApJ*, 579, 639
- Bond, I.A. 2001, *MNRAS*, 327, 868
- Boutreux, T., & Gould, A. 1996, *ApJ*, 462, 705
- Gaudi, B.S., & Gould, A. 1997, *ApJ*, 477, 152
- Gaudi, B.S., et al. 2002, *ApJ*, 566, 463
- Gould, A. 1992, *ApJ*, 392, 442
- Gould, A. 1995, *ApJ*, 421, L75
- Gould, A. 1995, *ApJ*, 441, L21
- Gould, A. 1999, *ApJ*, 514, 869
- Gould, A. 2000, *ApJ*, 542, 785
- Gould, A. 2004, *ApJ*, in press (astro-ph/0311548)
- Gould, A., Miralda-Escude, J., & Bahcall, J.N. 1994, *ApJ*, 423, L105
- Gould, A., & Salim, S. 1999, *ApJ*, 524, 794
- Mao, S. 1999, *A & A*, 350, L19
- Mao, S., et al. 2002, *MNRAS*, 329, 349
- Paczynski, B. 1986, *ApJ*, 304, 1
- Refsdal, S. 1966, *MNRAS*, 134, 315
- Schechter, P.L., Mateo, M., & Saha, A. 1993, *PASP*, 105, 1342
- Smith, M., Mao, S., & Paczynski, B., 2003, *MNRAS*, 339, 925

Smith, M., Mao, S., & Wozniak, P. 2002, *MNRAS*, 332, 962

Soszynski, I., et al. 2001, *ApJ*, 552, 731

van Belle, G. T. 1999, *PASP*, 111, 1515

Yoo, J., et al. 2004, *ApJ*, in press (astro-ph/0309302)

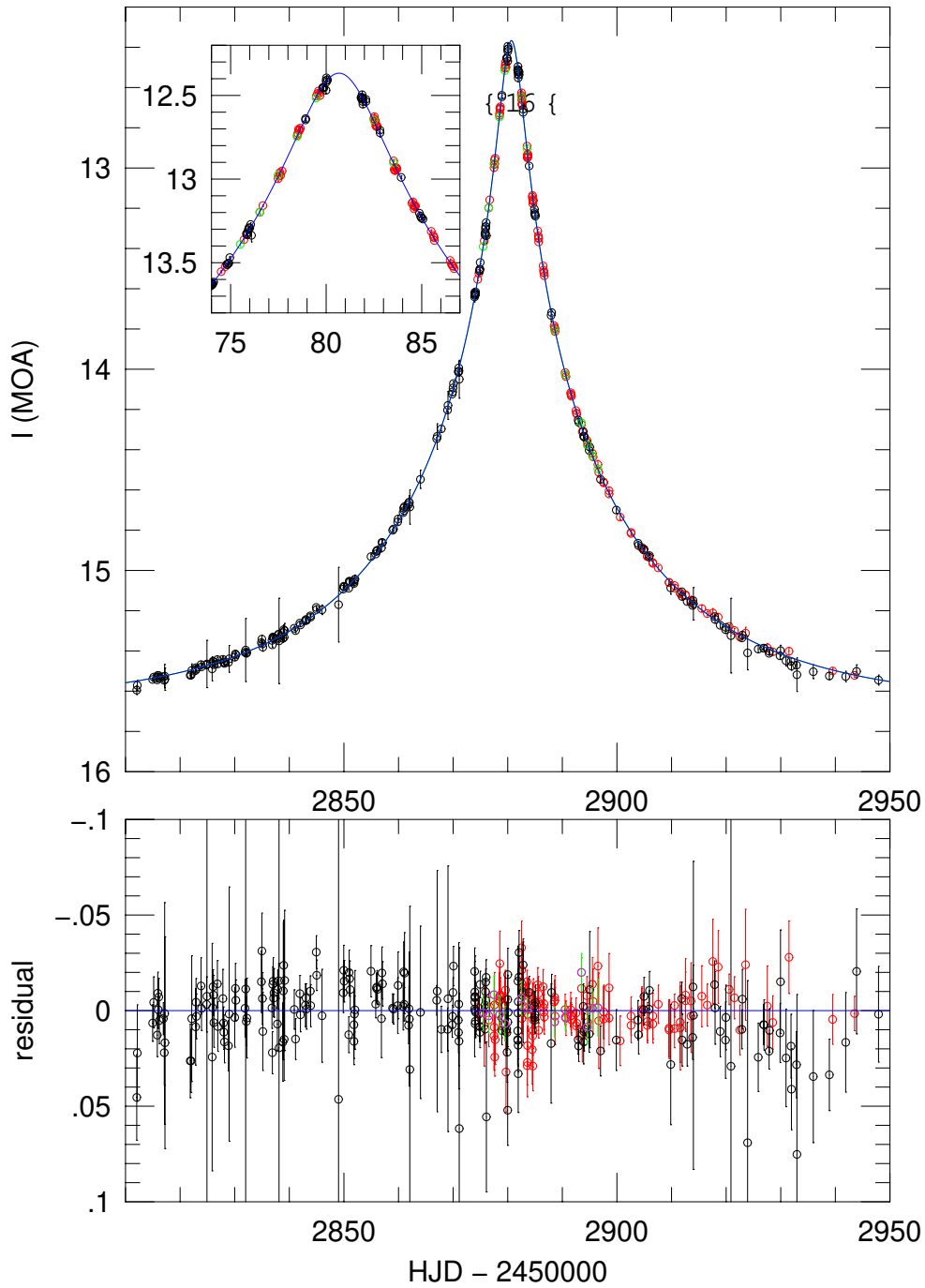


Fig. 1. Lightcurve of MOA 2003-BLG-37 showing data from MOA I (black), FUN I (red), and FUN V (green). The fit does not allow for parallax. The residuals show a very slight asymmetry, with the data brighter than the model on the rising wing and fainter on the falling wing. The MOA data are shown as recorded, and each FUN dataset has been linearly rescaled to be consistent with the MOA system. The MOA scale is not rigorously calibrated but is accurate to a few tenths of a magnitude.

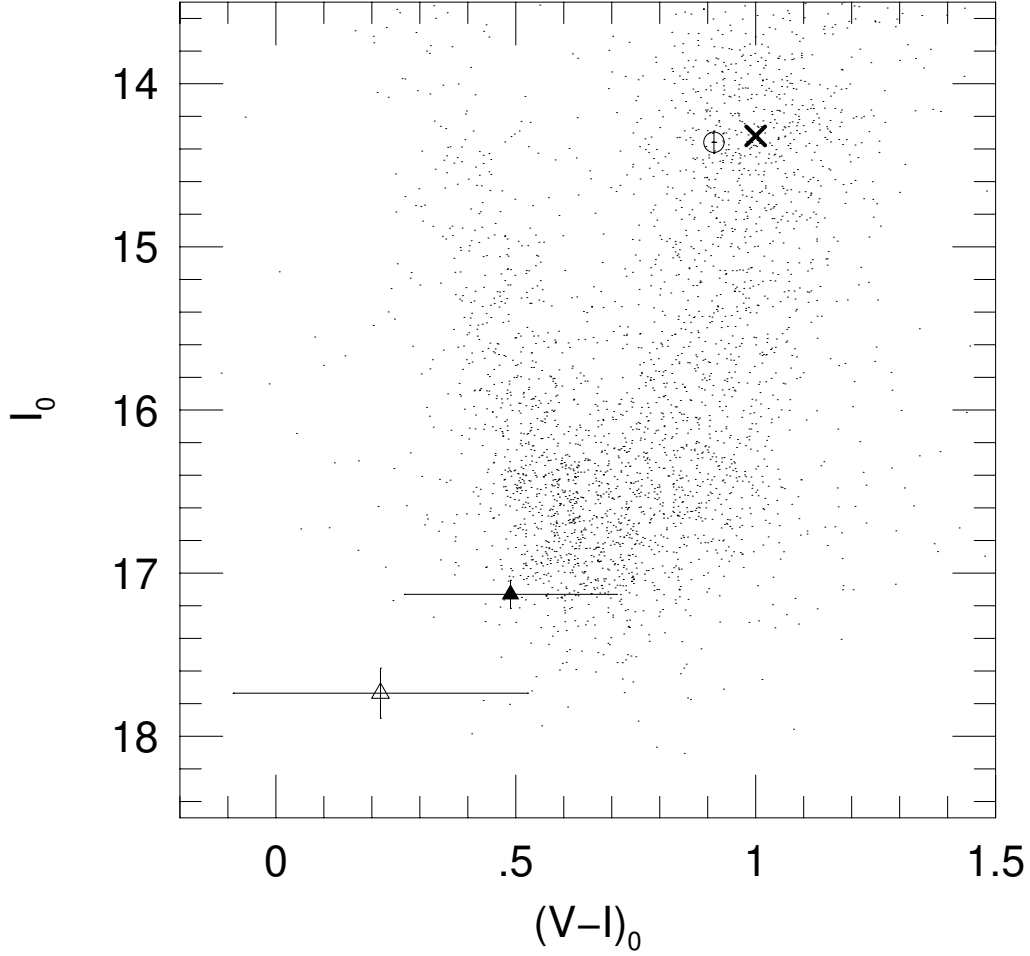


Fig. 2. Instrumental color-magnitude diagram of the $6^{\circ} \times 6^{\circ}$ field centered on MOA 2003-BLG-37. The diagram has been translated so that the centroid of the bulge clump giants (cross) is at its known position $[I_0; (V-I)_0]_{\text{clump}} = (14.32; 1.00)$. The open circle shows the color and magnitude of the (deblended) unblended source as determined from the fit to the lightcurve. Using this diagram and the standard technique described in Yoo et al. (2004), we find that the source has an angular radius of $\theta = 5.8 \pm 0.5$ as. The solid triangle shows the color and magnitude of the "hole" in the mottled background of bulge turn-off stars that is required to account for the negative blending in the no-parallax model. When parallax is included, the magnitude of this "hole" (open triangle) shrinks, and is more in line with what is expected.

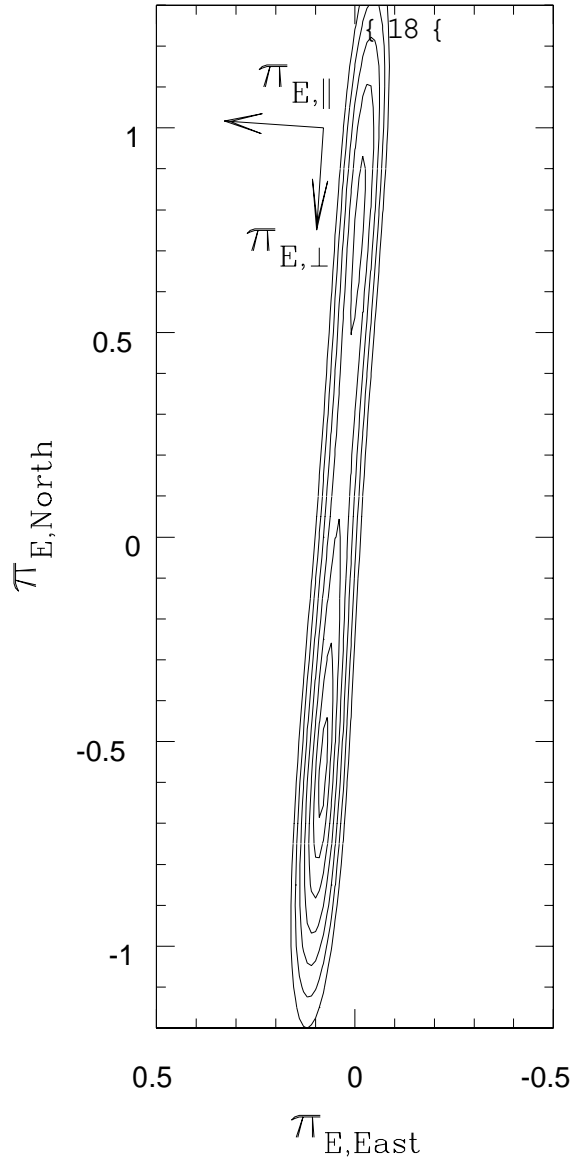


Fig. 3. Likelihood contours for the $u_0 < 0$ solutions in the microlens parallax (π_E) plane shown at $\chi^2 = 1, 4, 9, 16, 25, 36$, and 49 relative to the minimum. The magnitude of π_E gives the size of the Earth's orbit relative to the Einstein radius, and its direction is that of the lens-source relative motion. There are two local minima, with the northern minimum higher by $\chi^2 = 7.5$ and hence surrounded by the 3 contour. The two minima are embedded in contours of the continuous line-like degeneracy, which runs perpendicular to the direction of the Earth-Sun acceleration vector (arrows) and which reflects the parallax asymmetry. Note that since π_E is dimensionless, the axes have no unit labels. This diagram should be contrasted with figure 3 of Gould (2004) as described in § 5.1 of this paper.

Table 1. Jerk-Parallax Degenerate Solutions of MOA-2003-BLG-37

t_0 days	u_0	t_E days	$\pi_{E,N}$	$\pi_{E,E}$	$F_{s,\text{MOA}-I}$ (1)	$F_{b,\text{MOA}-I}$ (1)	$F_{s,\mu\text{FUN}-I}$ (2)	$F_{b,\mu\text{FUN}-I}$ (2)	$F_{s,\mu\text{FUN}-V}$ (3)	$F_{b,\mu\text{FUN}-V}$ (3)	χ^2
2880.6728	0.051488	42.5576	0.0000	0.0000	9.2533	-0.7179	29.1579	-2.2273	12.5789	-1.4197	753.093
2880.6791	-0.050506	43.5304	-0.5882	0.0818	9.0804	-0.5424	28.5826	-1.2718	12.3363	-1.0411	721.054
2880.6797	0.050509	42.9087	-0.5629	0.0872	9.0809	-0.5423	28.5853	-1.2748	12.3370	-1.0394	720.719
2880.6787	-0.050756	42.6415	0.7829	-0.0124	9.1258	-0.5932	28.7126	-1.4132	12.3949	-1.1167	728.594
2880.6778	0.050849	43.4089	0.7881	-0.0231	9.1426	-0.6111	28.7639	-1.4702	12.4168	-1.1392	730.522

Note. — 1 = In units of $I = 18$, where I is the (approximately calibrated) MOA apparent mag shown in Figure 1.

Note. — 2 = In units of $I_0 = 18$, where I_0 is the dereddened apparent mag used in Figure 2.

Note. — 3 = In units of $V_0 = 18$, where V_0 is the dereddened apparent mag used in Figure 2.